Available online at www.sciencedirect.com

ScienceDirect

Procedia Structural Integrity 39 (2022) 111–119

Structural Integrity Procedia

www.elsevier.com/locate/procedia

7th International Conference on Crack Paths

Crack paths for mild steel specimens with circular holes in high cycle fatigue

J. A. Balbín*, V. Chaves, C. Madrigal, A. Navarro

Departamento de Ingeniería Mecánica y Fabricación, Escuela Técnica Superior de Ingeniería, Universidad de Sevilla. Camino de los Descubrimientos s/n, Sevilla. 41092. España.

Abstract

The most common current models for predicting the fatigue limit in notched solids use the stresses along a straight line, beginning at the notch root, to make the prediction. This line represents a simplification of the path of a real crack, which usually has a first part, known as stage I, in the direction of the maximum tangential stress, and a second part, known as stage II, in the direction perpendicular to the maximum normal stress. In this work, experimental crack paths for notched solids are analysed, with the objective of establishing the directions and lengths of stages I and II of fatigue crack growth from notches. The material was a mild steel, the geometry of the specimen was a thin-walled tube with a passing-through hole and the tests were axial, with R = -1. From the tests, the S-N curves were constructed and the fatigue limits were calculated. For the high cycle fatigue tests, the cracks paths were studied, with special attention to the crack initiation point and the crack direction along the first grains. The cracks paths on the specimen outer surface were studied with an optical microscope. In this surface, the crack initiation point was close to the maximum principal stress point at the hole contour. The direction of the crack in the first and second grain showed great variability. This variability noticeably decreased as the crack reached a length of 10-20 grains, approaching the direction of Mode I. However, the crack might actually start at an interior point on the surface of the hole, which has a depth of 1500 μm. In fact, the point of maximum principal stress of the entire specimen is not at the specimen outer surface but on the internal surface of the hole at 750 μm from the outer surface, that is, half the thickness of the specimen. The crack path in the plane transverse to the hole containing this point of maximum principal stress was analysed. For this, the fracture surfaces, at both sides of the hole, were analysed with a non-contact 3D optical profiler. The crack path in this internal transverse plane followed the trend described for the crack path on the specimen outer surface: the initiation point close to the maximum principal stress point at the hole contour, great variability in the direction of the crack along the first grains and tendency to Mode I direction when the crack gets longer.

Keywords: Crack path; Notch; High cycle fatigue; Crack initiation point; Crack direction

* Corresponding author. Tel.: +34-954487311; fax: +34-954487295.
E-mail address: jbalbin@us.es

10.1016/j.prostr.2022.03.079

Nomenclature

d	diameter of circular hole
s	cross section diameter
D	Average material grain size
E	Young´s modulus
F	Force applied to specimen in fatigue tests
L	El-Haddad parameter
N	Fatigue life cycles
R	Stress ratio
σ	Applied stress amplitude
σ_{UTS}	Ultimate tensile strength
σ_{ys}	Yield strength
σ_{FL}	Endurance limit
θ	Crack initiation point angle
$\theta_{Ix'}$	Crack direction angle

1. Introduction

In polycrystalline materials, such as metals, fatigue crack initiation generally occurs near the planes of maximum shear stress, i.e. in the mode II direction, whereas crack propagation occurs near the plane perpendicular to the maximum tensile stress, i.e. in the mode I direction. These two phases of the crack growth are commonly referred to as *stage I* and *stage II* of fatigue crack growth, respectively, which were analyzed in depth by Forsyth (Forsyth (1962, 1969)). In (Forsyth (1962)), it is shown an excellent photograph for a pure cold rolled aluminium alloy, in which these two phases are clearly observed. The stage I to stage II transition is not yet well established.

The presence of a notch, from where the crack generally initiates, might modify the stages I and II of fatigue crack growth. There are several experimental studies in the literature about the crack direction during the initial period of crack growth in notched solids, and it is difficult to draw definitive conclusions from them: Meneghetti et al. studied low carbon steel plates weakened by U-notches (Meneghetti et al. (2007)) tested under axial cyclic loading and the crack paths were inspected with a microscope. The angle of crack initiation ranged from 16º to 30º and the average value was equal to about 25º. Berto et al. tested circumferentially V-notched specimens made of hardened and tempered steel and some run-out specimens were sectioned in the longitudinal direction and the paths of non-propagating cracks were examined (Berto et al. (2011)). As seen in two pictures of the article, for two axial loading tests, the cracks had approximately the mode I direction from their beginning. Lorenzino and Navarro tested Al1050 aluminium alloy plates with a circular hole under axial loading (Lorenzino and Navarro (2015)). The material had a large grain size, with the notch size of the same order or even smaller than the grain size. They studied the cracks growing from the hole on the two specimen surfaces with two optical microscopes and found that the crack paths were very irregular in their initial part, corresponding to the first grains, being highly affected by the microstructure of the material. Based on these results from the literature, it is difficult to establish what direction of the early crack path is expected in the presence of a notch.

In addition, these literature experimental studies analyzed the crack initiation direction on the outer surface of the specimens and, in the case of the work of Berto et al., in a longitudinal section of the cylindrical specimens. But it is likely that the crack started somewhere inside the specimen and not on the outer surface or in a different section from the one studied. This implies that the directions studied in these works may not be exactly representative of the crack initiation directions. In recent years there has been a great advance in the field of microscopy. Specifically, a 3D profiler has been used in a recent experimental campaign to analyze the fracture surfaces of notched fatigue tested specimens and to provide the evolution of the crack direction in the internal planes of the specimens, and not only in the plane of the outer surface of the specimen. It allows a more precise knowledge of stages I and II of fatigue crack

growth from notches. This experimental campaign began with a study on AISI 304L stainless specimens (Chaves et al. (2017)) and continued with 7075 aluminium alloy specimens (Chaves et al. (2019)). The present document reports the experimental study on a third material, a mild steel.

2. Material and tests

The material used in this work is commercial low carbon S355 steel (also known as St52). Its chemical composition (% weight) is: 0.18 C, Mn 1.28, Si 0.30, P 0.03, S 0.02, Cr 0.18, Ni 0.06, Al 0.025, Mo 0.01. The average grain size is 33 μm. No heat treatment is applied after the machining of the specimens. The monotonic properties, as determined from 20 tensile tests, are as follows: σ_{UTS} = 586 MPa, σ_{YS} = 412 MPa, E = 208 GPa. Vickers hardness equals to 187.9 HV.

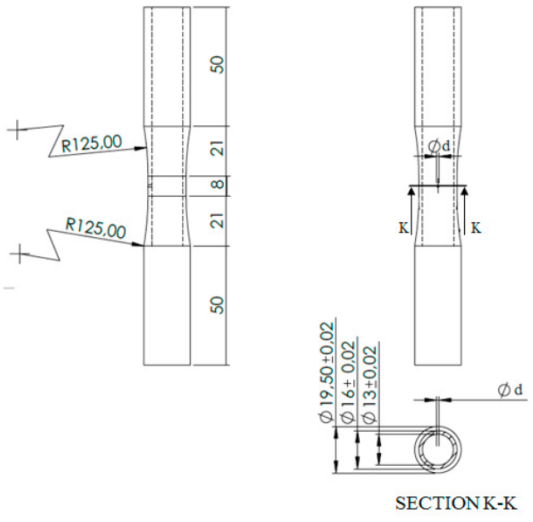

Fig. 1. Geometry of the specimens used for fatigue tests.

Firstly, fatigue tests under fully-reversed axial loading (R=-1) were conducted on smooth cylindrical specimens. The results were used to construct stress-life S-N curves in accordance with ASTM E739. The endurance limit at 10^6 cycles, expressed in terms of stress amplitude, was σ_{FL}= 275 MPa, calculated by the expression $\sigma = 4 \cdot F/(\pi \cdot s^2)$.

Then, axial fatigue tests were done using notched specimens. The geometry of the notched specimen is a thin-walled tube of 1500 μm thickness with a passing through hole in the central section. The diameter of the hole is d = 1.5 mm. Fig. 1 shows the geometry of the specimen. These specimens have been tested in a resonance fatigue testing machine, at approximately 150 Hz for fully-reversed axial loading (R=-1). A stress-life S-N curve has been constructed for the plain and notched specimen, finally having two S-N curves. Results are shown in Fig. 2 where stress values are referred to net section.

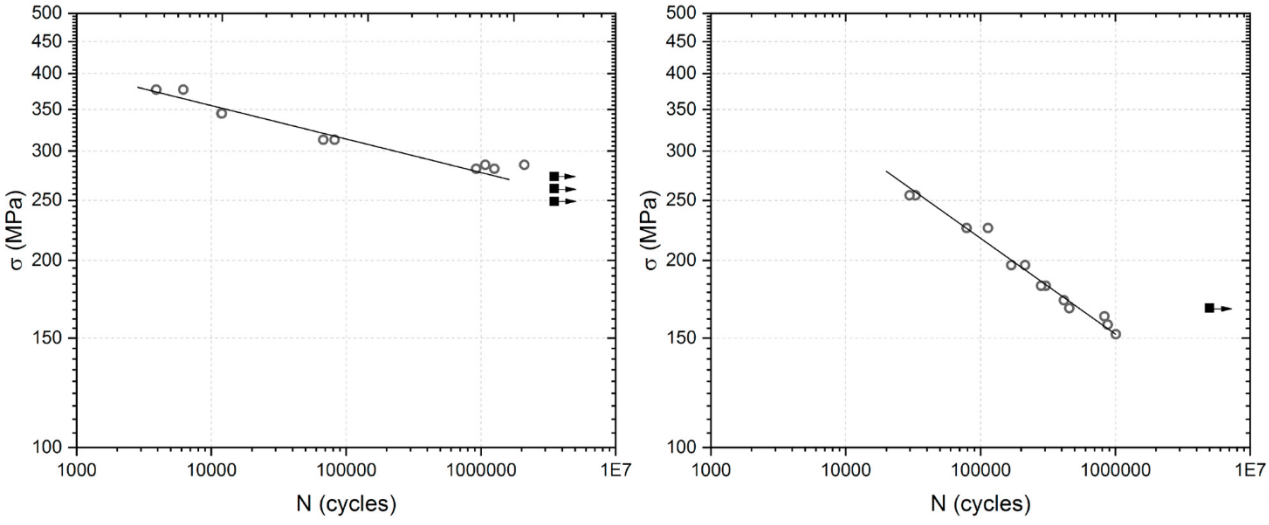

Fig. 2. Axial loading S-N curves for a) plain specimens and b) circular hole notched specimens d = 1.5 mm.

3. Crack paths

In this work, special attention has been paid to the experimental point of crack initiation and the crack direction path, primarily during the first period of crack growth, as some models base their evaluations on stresses along a line that is supposed to be representative of the crack path. This work deals with the experimental measurement of the crack initiation point and the crack direction not only at the outer surface but also at the specimen's mid-thickness plane. Angle measurements of crack initiation point and crack direction have been only performed in those specimens belonging to the high cycle fatigue regime, that is specimens broken beyond 10^5 cycles. Fig. 3a shows the axes layout where the origin of the coordinate system *OXYZ* is located on the outer surface of the specimen in the centre of the hole. The X-axis is in the central transverse section of the specimen, the Y-axis runs along the longitudinal dimension of the specimen and the Z-axis coincides with the axis of the hole. The location of the crack initiation point at the hole contour and the crack direction at some specific distances from the initiation point are determined through the angles θ and $\theta_{1x'}$, respectively. Figure 3b shows the geometrical definition of these two angles. The crack initiation point angle θ is measured over the X-axis from the centre of the hole. The crack direction angle $\theta_{1x'}$ is measured over an additional coordinate system o'*x'y'* whose origin coincides with the crack initiation point at the hole contour. This crack direction angle $\theta_{1x'}$ has been experimentally determined at several crack lengths, $a \approx \sqrt{\Delta x'^2 + \Delta y'^2}$, equal to some multiples of the average grain size, D, and also to some multiples of the El-Haddad parameter L (El Haddad et al. (1979)), that is 1, 2, 5, 10, 15 and 20 grains, and $L/2$, L, $2L$. After the angle measurements were taken, the subsequent analysis was carried out using the absolute values of these angles.

Regarding the crack at the outer surface of the specimen, Fig. 4 shows two cases of the experimental measurement of the crack initiation point angle θ. Most of the tested specimens show two opposite cracks growing from the hole. The crack initiation point is close to the maximum principal stress point at the hole contour (θ = 0º). The mean value of the angle θ for the studied specimens was 4,0º. Fig. 5, shows how the crack direction angle $\theta_{1x'}$ was measured. Table 1 shows the mean value of this angle $\theta_{1x'}$. A crack direction angle of 21,8º was found for a crack length of one average grain size, 1D, and a 14,7º angle for a crack length of two average grain sizes, 2D. These values certainly differ from Mode I and Mode II direction. Thus, the crack initiation direction seems to be mixed Mode direction. However, crack direction angles measured at larger crack lengths approach to Mode I direction. An example is a 4º angle obtained for a crack length of ten average grain sizes, 10D.

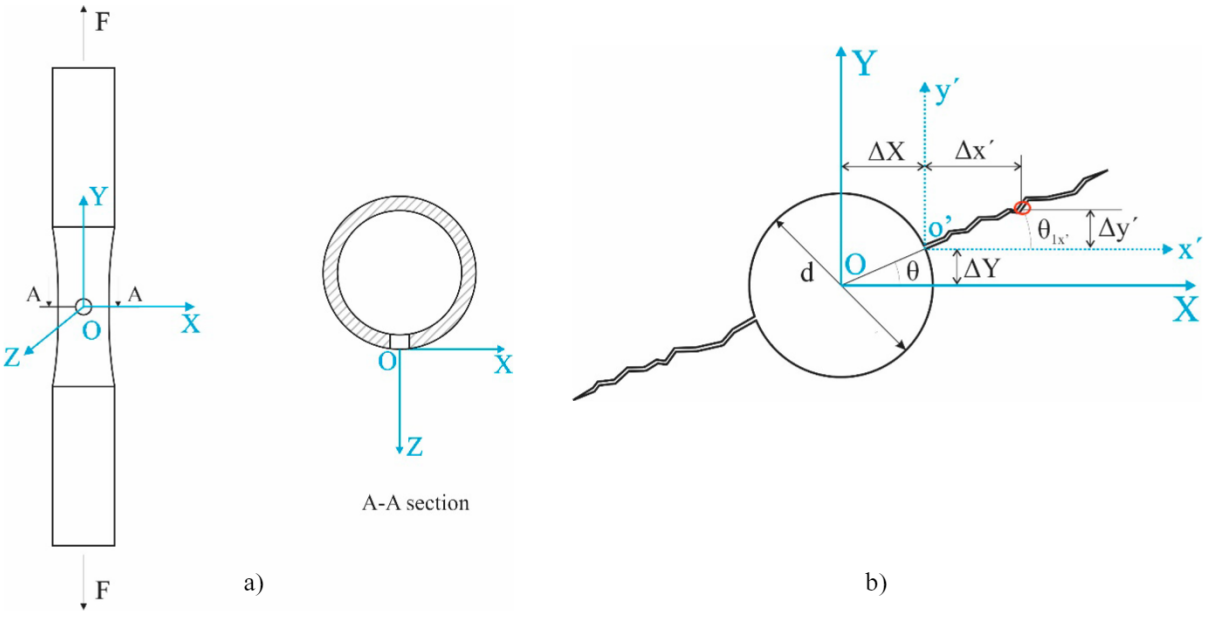

Fig. 3. a) Axes layout. b) Scheme of crack initiation point angle θ and crack direction angle $\theta_{1x'}$.

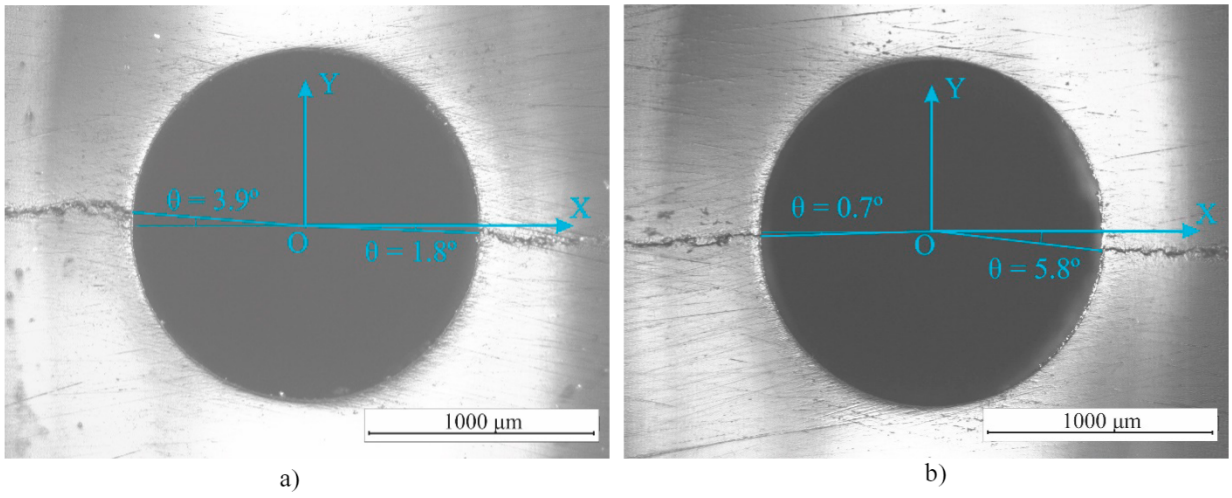

Fig. 4. Measurement of crack initiation point angles θ. a) N = 304400 cycles b) N = 415900 cycles.

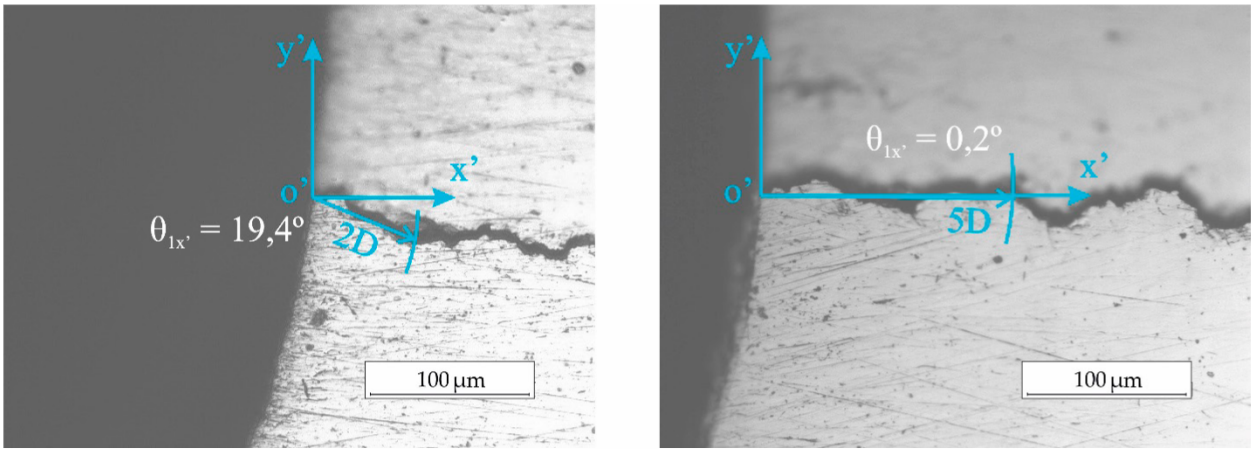

a) b)

Fig. 5. Crack path over the outer surface. Specimen broken after a) N = 455500 cycles b) N = 415900 cycles.

Table 1. Crack direction angle $\theta_{1x'}$ measured over the outer surface of the specimen.

Crack length	$a = 1D$	$a = 2D$	$a = 5D$	$a = 10D$	$a = 15D$	$a = 20D$	$a = L/2$	$a = L$	$a = 2L$
$\theta_{1x'}$	21,8°	14,7°	7,0°	4,0°	2,5°	1,7°	9,3°	6,4°	3,8°

4. Analysis of the fracture surfaces

In a previous work (Chaves et al. (2019)), a linear elastic stress analysis of the specimen shown in Fig. 1 was performed using the finite element software ANSYS v. 15.0 (ANSYS). The point of maximum principal stress was located at the hole surface and at the mid-thickness plane of the specimen (Z = -750 µm). Because of that, the crack initiation point and the crack direction were also evaluated at this Z = -750 µm plane, assuming that this is the most likely plane to find the crack initiation. To do that, an analysis of the fracture surfaces at both sides of the hole were carried out using an optical microscope, a scanning electron microscope (SEM) and a non-contact 3D optical profiler. No clear crack initiation points were observed on the fracture surfaces, so a possible crack initiation at the mid-thickness plane (Z = -750 µm) might be justified.

The 3D topography of the fracture surfaces was captured using the optical profiler through Focus Variation technology, which is useful for measuring the shape of large rough surfaces. It also allows measurements including high slope surfaces (up to 86°), high measurement speed and large vertical range. An example of fracture surface near the hole is shown in Fig. 6a. The resolution is half a micron in the three coordinate axes. The points of the fracture surface with higher Y values are shown in red, blue points refer to lower Y values and black areas indicate steep slope. The intersection of the fracture surface with the mid-thickness plane Z = -750 µm results on the mid-thickness crack path (black line) shown in Fig. 6b. The angle θ measured on the outer surface of the specimen serves as the reference to obtain the value of the angle θ in the mid-thickness crack path. This calculation consists on a relation between the Y heights of the crack initiation point at Z = 0 µm and the crack initiation point at Z = -750 µm. The mean value of the angle θ for the studied specimens was 4,5°, which is very similar to value 4,0° reached on the outer surface of the specimen. Table 2 shows the mean value of the angle $\theta_{1x'}$. As done previously for the outer surface crack path, a crack

direction angle of 11,7º was found for a crack length of one average grain size, 1*D*, and an 8,2º angle for a crack length of two average grain sizes, 2*D*. These values also differ from Mode I and Mode II direction. Crack direction angles measured at larger crack lengths approach to Mode I direction again. An example is a 2,2º angle obtained for a crack length of ten average grain sizes, 10*D*.

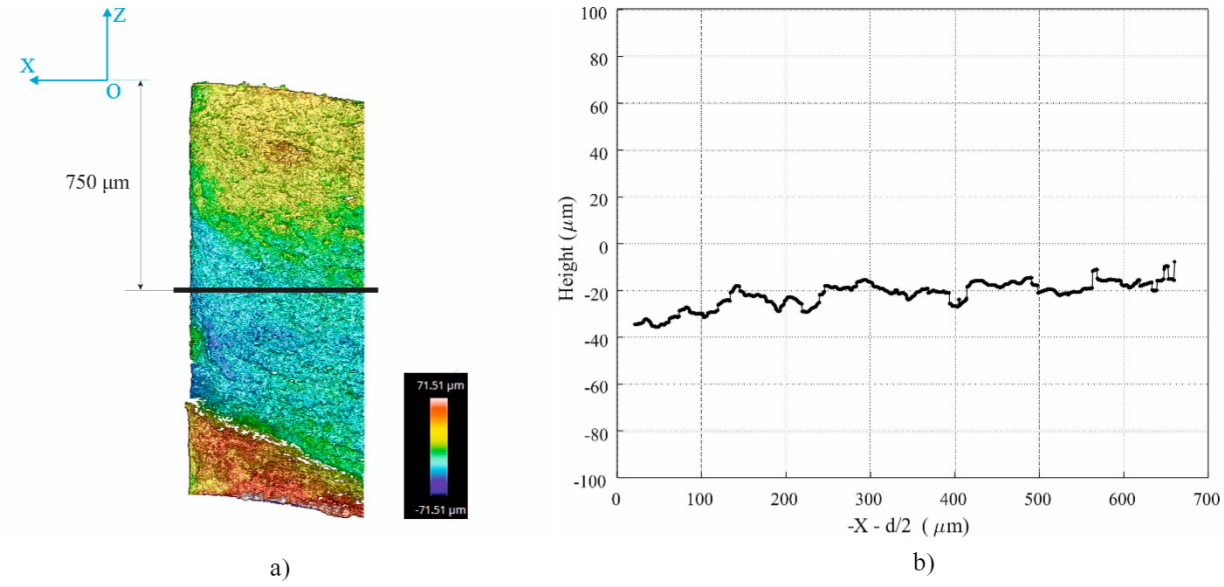

Fig. 6. a) Fracture surface and mid-thickness plane (Z = -750 µm) and b) heights of the crack path points.

Table 2. Crack direction angle $\theta_{Ix'}$ measured at the mid-thickness plane crack path (Z = -750 µm).

Crack length	$a = 1D$	$a = 2D$	$a = 5D$	$a = 10D$	$a = 15D$	$a = 20D$	$a = L/2$	$a = L$	$a = 2L$
$\theta_{Ix'}$	11,7º	8,2º	4,4º	2,2º	1,4º	1,1º	5,9º	4,0º	2,1º

Fig. 7 shows a comparison of the angle θ for both crack path locations (Z = 0 µm and Z = -750 µm). Results are similar in both planes as they are close to zero degrees which means that the initiation point at the hole contour is very close to the maximum principal stress point. Fig. 8 shows the angle $\theta_{Ix'}$ for both crack path planes. Results are similar and show the same trend. It can be seen a great variability along the first and second grains. After that, the angle $\theta_{Ix'}$ tends to Mode I direction (10-20 grains, e.g.) since it approaches to zero degrees value.

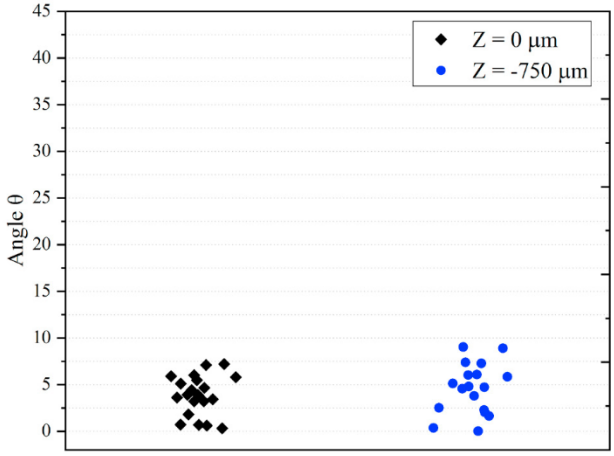

Fig. 7. Crack initiation point angles.

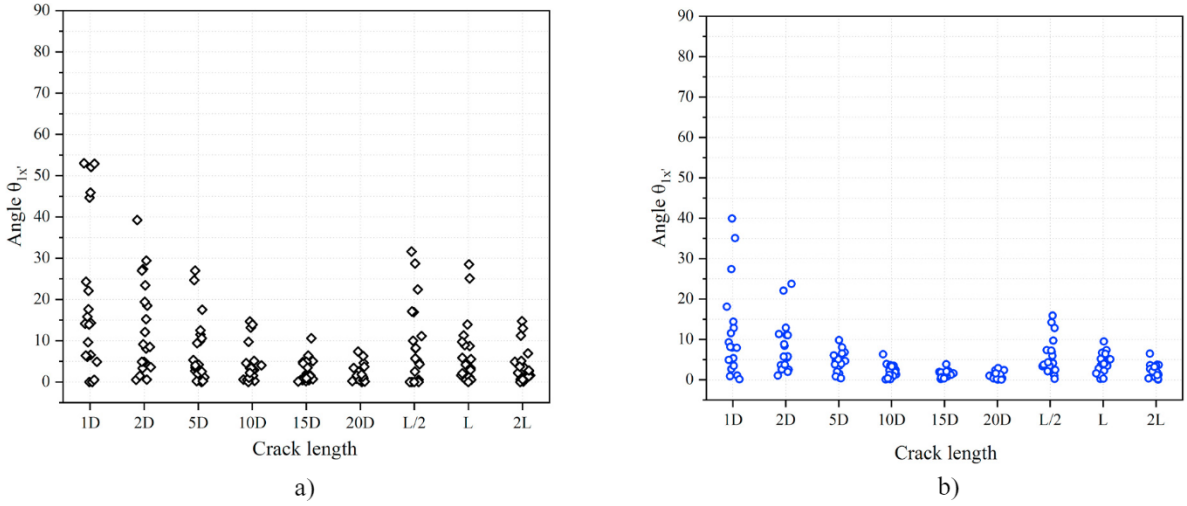

Fig. 8. Crack direction angles measured at a) outer surface (Z = 0 µm) and at b) mid-thickness plane (Z = -750 µm).

5. Conclusions

S-N curves were constructed for low carbon steel specimens with a circular hole and subjected to axial loading (R=-1). For specimens broken in the high cycle fatigue regime, the crack paths growing from the hole were studied with an optical microscope, a non-contact 3D profiler and SEM equipments. The crack initiation point and the crack direction were analysed in two planes: one at the outer surface of the specimen and another at an internal plane located at the mid-thickness of the specimen. The results show similar trend for both planes. The crack initiation point was close to the maximum principal stress point at the hole contour. The crack initiation direction followed a mixed Mode direction, between Mode I and Mode II direction. Crack propagation direction approached the Mode I direction.

Acknowledgements

The authors would like to thank the European Union, the Spanish Government and the Junta de Andalucía for its financial support through grants DPI2017-84788-P (FEDER/Ministerio de Ciencia e Innovación - Agencia Estatal de Investigación) and P18-FR-4306 ("Fondo Europeo de Desarrollo Regional (FEDER) y Consejería de Economía, Conocimiento, Empresas y Universidad de la Junta de Andalucía, dentro del Programa Operativo FEDER 2014-2020").

References

ANSYS Mechanical APDL, Release 15.0.7.

Berto, F., Lazzarin, P., Yates, J.R., 2011. Multiaxial fatigue of V-notched steel specimens: a non-conventional application of the local energy method. Fatigue & Fracture of Engineering Materials & Structures, 34, 921–943.

Chaves V., Beretta G., Navarro A., 2017. Biaxial fatigue limits and crack directions for stainless steel specimens with circular holes. Engineering Fracture Mechanics, 174, 139-154.

Chaves, V., Beretta, G., Balbín, J.A., Navarro, A., 2019. Fatigue life and crack growth direction in 7075-T6 aluminium alloy specimens with a circular hole under biaxial loading. International Journal of Fatigue, 125, 222-236.

El Haddad, M.H., Topper, T.H., Smith, K.N., 1979. Prediction of non propagating cracks. Engineering Fracture Mechanics, 11 (3), 573-584.

Forsyth, P.J.E., 1962. A two stage process of fatigue crack growth. In: Proceedings of the crack propagation symposium, 1, 76-94.

Forsyth, P.J.E., 1969. The physical basis of metal fatigue. Blackie and son limited, London and Glasgow.

Lorenzino, P., Navarro, A., 2015. Growth of very long "short cracks" initiated at holes. International Journal of Fatigue, 71, 64-74.

Meneghetti, G., Susmel, L., Tovo, R., 2007. High-cycle fatigue crack paths in specimens having different stress concentration features. Engineering Failure Analysis, 14, 656-672.